Pten loss in the bone marrow leads to G-CSF–mediated HSC mobilization

Melania Tesio,[1,2] Gabriela M. Oser,[1,3] Irène Baccelli,[1,2] William Blanco-Bose,[3] Hong Wu,[4] Joachim R. Göthert,[5] Scott C. Kogan,[6] and Andreas Trumpp[1,2,3]

[1]Deutsches Krebsforschungszentrum (DKFZ), D-69120 Heidelberg, Germany
[2]Heidelberg Institute for Stem Cell Technology and Experimental Medicine (HI-STEM gGMBH), D-69120 Heidelberg, Germany
[3]Swiss Institute for Experimental Cancer Research (ISREC), School of Life Science, Ecole Polytechnique Fédérale de Lausanne (EPFL), 1015 Lausanne, Switzerland
[4]Department of Molecular and Medical Pharmacology, Eli and Edythe Broad Center of Regenerative Medicine and Stem Cell Research, University of California, Los Angeles School of Medicine, Los Angeles, CA 90095
[5]Department of Hematology, Universitätsklinikum Essen, Westdeutsches Tumorzentrum (WTZ), D- 45147 Essen, Germany
[6]Department of Laboratory Medicine and Comprehensive Cancer Center, University of California, San Francisco, San Francisco, CA 94143

The phosphatase and tumor suppressor PTEN inhibits the phosphoinositol–3–kinase (PI3K) signaling pathway and plays a key role in cell growth, proliferation, survival, and migration. *Pten* conditional deletion using MxCre or Scl–CreER[T] leads to splenomegaly and leukemia formation, which occurs after the relocation of normal hematopoietic stem cells (HSCs) from the bone marrow to the spleen. Unexpectedly, dormant HSCs in the bone marrow do not enter the cell cycle upon *Pten* loss, they do not lose self–renewal activity, and they are not exhausted. Instead, *Pten* deficiency causes an up–regulation of the PI3K pathway in myeloid cells, but not in HSCs. Strikingly, myeloid cells secrete high levels of G-CSF upon *Pten* loss, leading to the mobilization of HSCs from the bone marrow and accumulation in the spleen. After deletion of *Pten* in mice lacking G-CSF, the splenomegaly, myeloproliferative disease, and splenic HSC accumulation are rescued. Our data show that although PTEN has little if any role in normal HSCs, it is essential to prevent overt G-CSF production by myeloid and stromal cells which otherwise causes HSCs to relocate to the spleen followed by lethal leukemia initiation.

CORRESPONDENCE
Andreas Trumpp:
a.trumpp@dkfz.de

Abbreviations used: CRU, competitive repopulation unit; HSC, hematopoietic stem cell; KC, keratinocyte-derived chemokine; LRC, label retaining cell; MPD, myeloproliferative disease; pI-pC, polyinosine-polycytidine; T-ALL, T cell acute lymphoblastic leukemia/lymphoma; Tx, tamoxifen.

BM hematopoietic stem cells (HSCs) are multipotent cells that divide infrequently and, during homeostasis, are predominantly quiescent or even dormant. This dormant cell cycle status is thought to protect stem cells from acquiring mutations that may lead to the exhaustion of the HSC pool and/or the generation of putative cancer stem cells (Wilson et al., 2008; Essers and Trumpp, 2010; Baccelli and Trumpp, 2012; Doulatov et al., 2012). The underlying mechanism of quiescence in HSCs is likely mediated by the various BM stem cell niches comprised of multiple different cell types (Ehninger and Trumpp, 2011; Yamazaki et al., 2011; Ding et al., 2012; Lander et al., 2012; Park et al., 2012). Several signaling molecules, including TGF-β, Thrombopoietin, Angiopoietin-1, and CXCL12 (SDF-1), have been shown to be secreted by niche cells and maintain HSC quiescence by inhibiting HSC cycling (Arai et al., 2004; Sugiyama et al., 2006; Yamazaki et al., 2006, 2011; Qian et al.,

2007; Yoshihara et al., 2007). In addition, transcription factors, such as c-Myc, and FoxOs, as well as CDK inhibitors (p18[Ink4c], p21[CIP1], and p57[Kip2]) have also been suggested to regulate the balance between HSC quiescence and self-renewal (Wilson et al., 2004; Yu et al., 2006; Tothova and Gilliland, 2007; Orford and Scadden, 2008; Matsumoto et al., 2011; Tesio and Trumpp, 2011; Zou et al., 2011). Quiescent cells are driven into cell cycle in response to hematopoietic stress conditions. Stress-induced cytokines, including type I and II IFNs and G-CSF, all promote dormant HSCs to enter an active cell cycle mode (Tothova and Gilliland, 2007; Wilson et al., 2008; Essers et al., 2009; Baldridge et al., 2010).

PTEN encodes a phosphatase that negatively regulates intracellular levels of phosphatidylinositol–3,4,5–trisphosphate (PIP3) and

M. Tesio and G.M. Oser contributed equally to this paper.

The Rockefeller University Press $30.00
J. Exp. Med. 2013 Vol. 210 No. 11 2337–2349
www.jem.org/cgi/doi/10.1084/jem.20122768

2337

functions as a tumor suppressor by negatively regulating the Akt/PKB signaling pathway. It dephosphorylates the phospholipid PIP3 to produce PIP2, and thus it is a direct antagonist of PI3 kinase (PI3K). Previous studies have shown that both PI3K-AKT–dependent and –independent signaling pathways are regulated by PTEN (Vivanco et al., 2007; Gu et al., 2011; Kalaitzidis et al., 2012; Magee et al., 2012). Loss of PTEN function typically leads to an increase in PI3K signaling, causing hyperplasia and tumorigenesis such as glioblastoma, prostate cancer, or T cell leukemias (Knobbe et al., 2008; Song et al., 2012). Previous studies have proposed that the absence of PTEN activity promotes the generation of leukemic stem cells by driving unlimited self-renewal. In contrast to the leukemic situation, it was suggested that loss of *Pten* in the hematopoietic system leads to the apparent depletion of normal HSCs from the BM (Yilmaz et al., 2006; Zhang et al., 2006; Lee et al., 2010; Magee et al., 2012). Thus, it was proposed that PTEN plays opposite roles in normal HSCs and leukemic stem cells with respect to self-renewal, although the mechanism for this phenomenon still remains enigmatic. In this study, we use two conditional *Pten* loss-of-function mouse models to show that the mobilizing cytokine G-CSF is overproduced in the absence of *Pten*, which has widespread consequences for the balance of the hematopoietic system.

RESULTS

Conditional elimination of the *Pten*flox allele by SCL–CreERT

Previous studies investigated the role of PTEN in HSCs using the Mx1-Cre (MxCre) model carrying the IFN-α inducible Mx1 promoter, which is activated by injecting mice with polyinosine-polycytidine (pI-pC) to induce high levels of IFN-α. However, in this model, it cannot be excluded that the type I IFN signaling cascade, activated in parallel to Cre-mediated *Pten* deletion, might cross talk or synergize with the hematopoietic effects upon *Pten* loss (Essers et al., 2009). To circumvent this issue, we generated a new genetic mouse model where *Pten* deletion is driven by the tamoxifen (Tx)-inducible Scl-CreERT allele (Scl-Cre). In this model, the Scl-Cre allele efficiently recombines floxed alleles in hematopoietic stem/progenitors and (to a lesser degree) in endothelial cells (Fig. 1 A; Göthert et al., 2005), thus allowing the assessment of PTEN function in HSCs independently of IFN-α.

Experimental (Scl-CreERT;*Pten*fl/fl) and littermate control mice (*Pten*fl/fl) were fed with a Tx diet starting at 4–5 wk of age. As expected, the *Pten* gene and PTEN protein were eliminated from the BM and spleen of mice, which, after Cre induction are referred to as *Pten*ΔScl (Fig. 1 B and not depicted).

We then compared our new *Pten* conditional KO model to the MxCre model in which MxCre;*Pten*fl/fl and littermate control mice (*Pten*fl/fl) were injected with pI-pC every other day for a total of five doses. As shown in Fig. 1 (B and C), an efficient elimination of *Pten* gene and PTEN protein was achieved in the BM and spleen of mice, which after
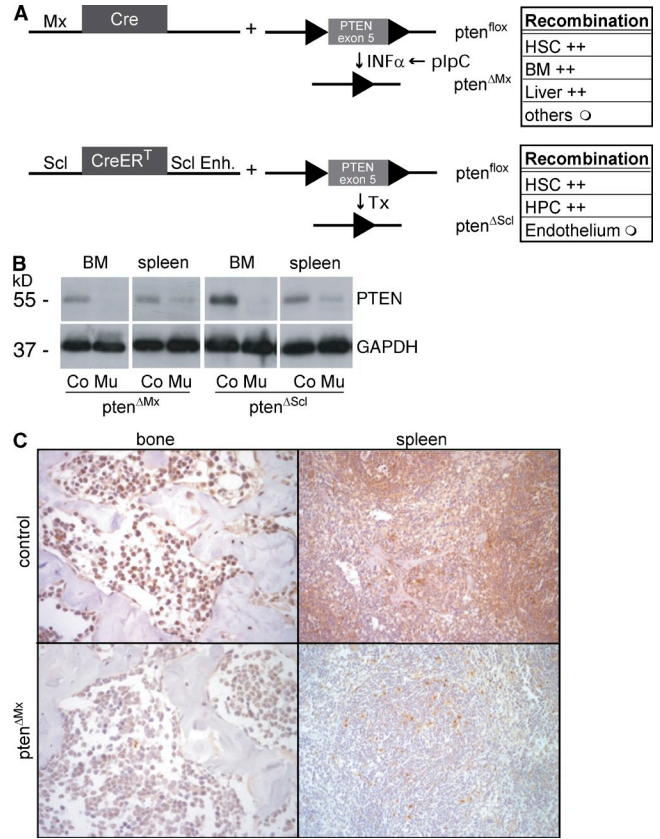

Figure 1. Conditional elimination of the *pten*flox allele in the hematopoietic system using SCL–CreERT and Mx-Cre. (A) Schematic diagram of the two conditional KO approaches and description about the tissue-specific recombination efficiency (right); +, >90%; ○, <50%. (B) Western blot showing the efficiency of *Pten* elimination in BM and spleen. (C) Analysis of *PTEN* expression in sections of bone and spleen using immunohistochemistry. Representative figures (bone, 1 cm = 250 µM; spleen, 1 cm = 500 µM) are shown. The data presented are representative of least three different independent experiments.

MxCre-mediated deletion are referred to as *Pten*ΔMx (not depicted). Our results also indicate that the two conditional KO models delete *Pten* with a similar efficiency.

*Pten*ΔScl mice develop myeloproliferative disease (MPD) and T cell acute lymphoblastic leukemia/lymphoma (T–ALL)

In *Pten*ΔMx mice, lethality occurs, on average, 7.5 wk after the first pI-pC injection. In contrast, *Pten*ΔScl mice lived significantly longer with a median survival of 16.5 wk (Fig. 2 A). Similar to what has been previously reported after MxCre-mediated *Pten* deletion, *Pten*ΔScl mice also displayed splenomegaly (Fig. 2 C). Pathological analysis of the morphology of hematopoietic organs revealed extramedullary hematopoiesis and MPD in the spleen, and granulocytic hyperplasia in the bones of both types of *Pten* mutant mice (Fig. 2 D). In agreement with the MPD pathology, immature myeloid CD11b+/Gr1+ cells were increased in mutant spleens (Fig. 2, D and E). Consistently, in these populations *Pten* was efficiently deleted in BM and spleen. As a consequence, increased phosphorylation
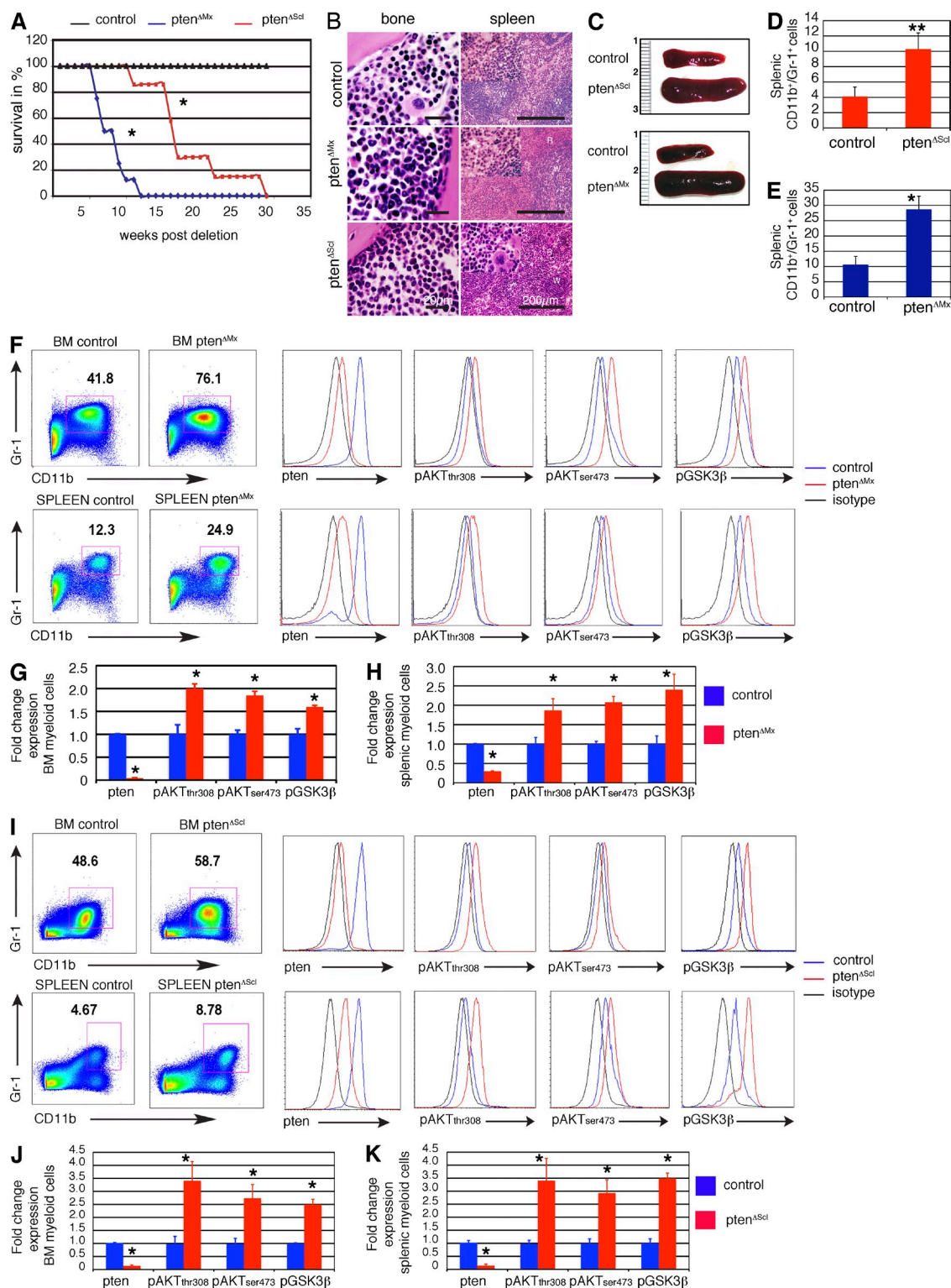
Figure 2.   Elimination of Pten using SCL–CreER^T causes premature lethality. (A) Kaplan-Meyer analysis showing lethality upon *Pten* deletion in *Pten*^ΔMx and *Pten*^ΔScl mice. P < 0.05. *n* = 6 mice each group. (B) Hematoxylin & Eosin (H&E)–stained histological sections of bone and spleen showing MPD in the spleen and granulocytic hyperplasia in the bone. R, red pulp; W, white pulp. Bars: (spleen) 200 µm; (bone) 20 µm. (C) Splenomegaly in *Pten*^ΔMx and *Pten*^ΔScl mice 4 and 7 wk after deletion, respectively. (D) Splenic CD11b⁺Gr-1⁺ cells in control or *Pten*^ΔScl mice. Three independent experiments, *n* = 7 controls and *n* = 6 mutants. ** indicates statistically significant change, P = 0.001. (E) Splenic CD11b⁺Gr-1⁺ cells in control or *Pten*^ΔMx mice. Three independent experiments, *n* = 8 each group. P = 0.029. (F–H) *Pten*, pAktTh308, pAktSer473, and pGSK3βSer9 levels in BM (top) and splenic (bottom) CD11b⁺Gr-1⁺ cells
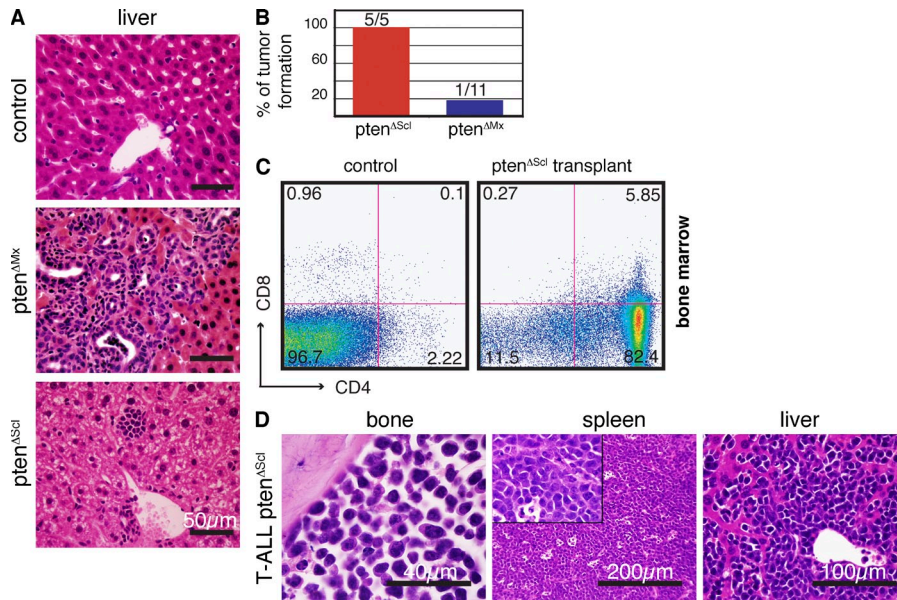
Figure 3. **Elimination of Pten using SCL–CreER^T induces leukemia.** (A) H&E-stained histological sections of livers from $Pten^{\Delta Mx}$, $Pten^{\Delta Scl}$, or control mice. (B) Frequency of tumors in NOD/SCID mice after transplantation of 10^6 BM cells of sick $Pten^{\Delta Scl}$ mice and $Pten^{\Delta Mx}$, $n = 5$ and $n = 11$, respectively. Data are provided as mean ± SE. (C) FACS profile showing CD4 and CD8 expression in the BM of a control NOD/SCID mouse (left) and a $Pten^{\Delta Scl}$ transplanted NOD/SCID mouse (right). (D) H&E-stained histological sections of bone, spleen, and liver of a typical $Pten^{\Delta Scl}$ mouse showing T-ALL.

of AKT (on Thr308 and Ser437) and GSK3β was detected in both models, consistent with an activated PI3K–AKT signaling pathway (Fig. 2, F–K; Cross et al., 1995).

Intriguingly, in contrast, to $Pten^{\Delta Mx}$ mice, all $Pten^{\Delta Scl}$ animals developed T-ALL as early as 12 wk after deletion (Fig. 3, A–D), similar to VEC-Cre–mediated $Pten$ deletion in fetal liver HSCs (Guo et al., 2008). Transplantation of BM isolated from sick $Pten^{\Delta Scl}$ mice caused 100% of NOD/SCID recipients (5/5) to die of CD4$^+$ T-ALL after 3–6 wk (Fig. 3, B and C). In contrast, only 9% of the recipient mice (1/11) transplanted with the BM of sick $Pten^{\Delta Mx}$ mice developed T-ALL (Fig. 3 B). This indicates that $Pten^{\Delta Mx}$ BM also contains some premalignant or even malignant T-ALL clones, albeit at lower frequencies than in $Pten^{\Delta Scl}$ BM. The reduced T-ALL malignancy detected in $Pten^{\Delta Mx}$ mice may be related to the liver disease of $Pten^{\Delta Mx}$ mice early on, which likely prevents the development of a full-blown T-ALL leukemia. In summary, in addition to being an important negative regulator of myelopoiesis, PTEN is predominantly a tumor suppressor for T cell leukemia and $Pten^{\Delta Scl}$ animals serve as a novel highly penetrant model of T-ALL to identify interacting pathways and to design and test novel therapeutic approaches.

HSC quiescence is not compromised in the BM of $Pten^{\Delta Scl}$ and $Pten^{\Delta Mx}$ mice

We then analyzed the HSC compartment (defined here as lineage^{neg}Sca1$^+$cKit$^+$ [LSK] CD34$^-$CD135$^-$) of both $Pten^{\Delta Scl}$ and $Pten^{\Delta Mx}$ mice. In agreement with previous reports (Chen et al., 2006; Yilmaz et al., 2006), we observed a decrease of BM HSCs over time in both $Pten^{\Delta Scl}$ and $Pten^{\Delta Mx}$ animals (Fig. 4 A). However, unexpectedly, no significant differences in the frequencies of quiescent (Ki67^{neg}) or cycling (BrdU$^+$ and/or Ki67$^+$) HSCs were detected in either model (Fig. 4, B and E). Because these analyses only measure the immediate cell cycle status and may therefore not be sensitive enough to discriminate between infrequently dividing and dormant HSCs, we analyzed the frequency of dormant label retaining cells (LRCs; Wilson et al., 2008). After an initial 10–d labeling period, BrdU was removed and $Pten^{\Delta Scl}$ and control $Pten^{fl/fl}$ mice were switched onto a Tx diet for 21 d, followed by additional 49 d of chase. Analysis of the percentage of BrdU$^+$LRC cells within the HSC compartment revealed not a decrease as expected, but an increase of LRCs-HSCs in $Pten^{\Delta Scl}$ mice (Fig. 4 C). In summary, these data suggest that $Pten$ deficiency does not alter the cell cycle distribution of primitive HSCs. Accordingly, the expression profile of control and $Pten$-deficient HSCs did not reveal significant differences in genes involved in cell cycle control (unpublished data). Finally, to further examine whether functional HSCs may show a differential proliferative behavior in the absence of $Pten$, mice were treated weekly with the chemotherapeutic agent 5-FU. As shown in Fig. 4 D, similar lethality kinetics in $Pten^{\Delta Scl}$, $Pten^{\Delta Mx}$, and control mice was observed, suggesting a similar proliferative index of HSC/P in $Pten$ mutants and WT littermates. In conclusion, using the currently available methods to analyze the cell cycle of HSCs in vivo, we could not identify

of $Pten^{\Delta Mx}$ and control counterparts pI-pC injected for 15 d. Data were obtained using a detergent-based protocol (Cytofix/Cytoperm; BD). A representative FACS plot (F) and the fold change in the expression levels (G and H) are shown. Three independent experiments, $n = 6$ controls and $n = 4$ mutants. P < 0.05 for all stainings of BM and spleen. (I–K) $Pten$, pAktTh308, pAktSer473, and pGSK3βSer9 levels in BM (top) and splenic (bottom) CD11b$^+$Gr-1$^+$ cells of $Pten^{\Delta Scl}$ and control counterparts fed with Tx diet for 28 d. Data were obtained using a detergent-based protocol (Cytofix/Cytoperm). A representative FACS plot (I) and the fold change in the expression levels (J and K) are shown. Three independent experiments, $n = 6$ each group. P < 0.05 for all stainings of BM and spleen. Data are provided as mean ± SE. Unless otherwise indicated, * indicates statistically significant change with P < 0.05.
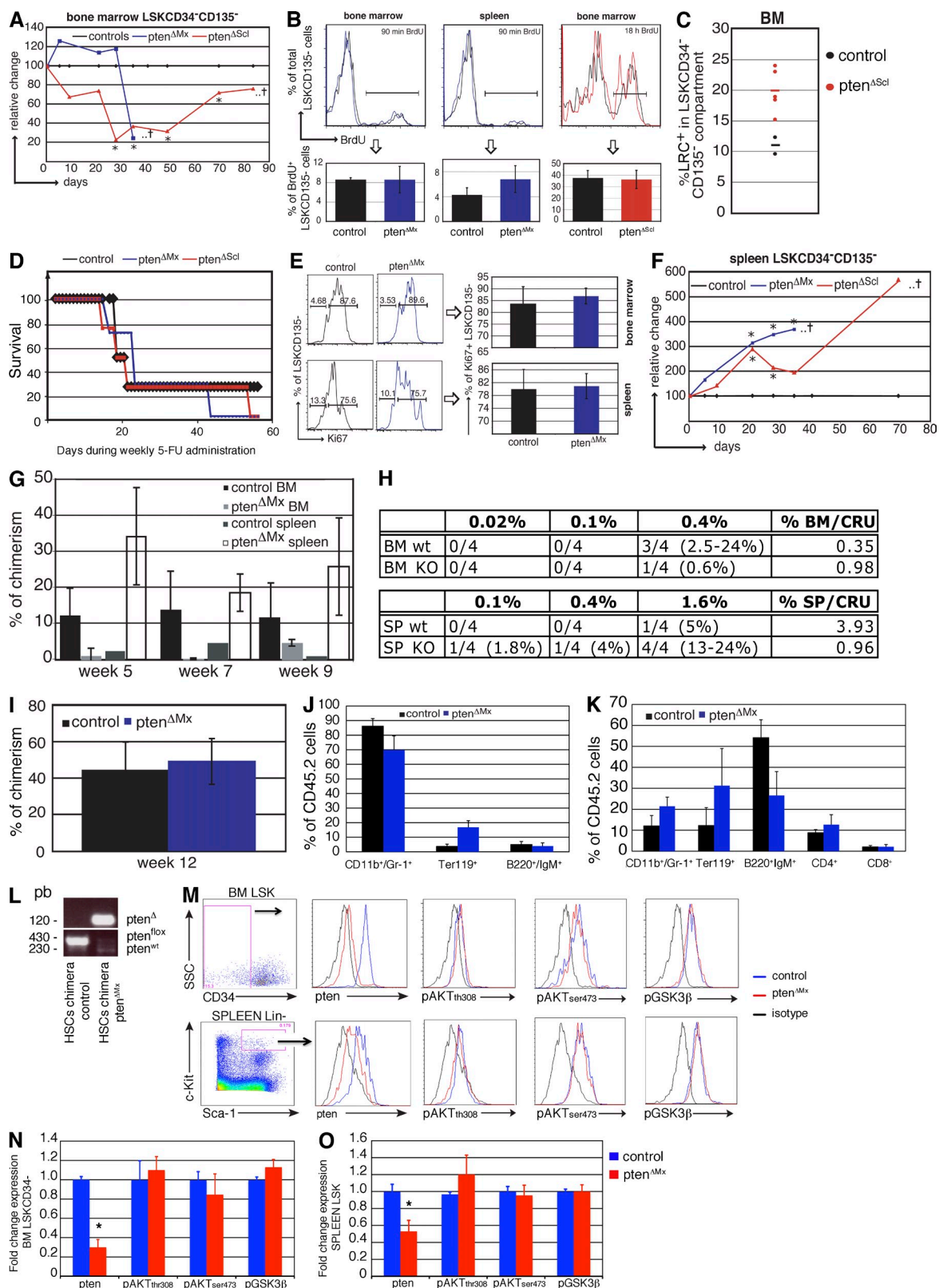
Figure 4. Phenotypic and functional analysis of Pten–deficient HSCs. (A) Kinetic analysis of the relative change of LSKCD34⁻CD135⁻ cells in the BM of *Pten*^ΔMx and *Pten*^ΔScl mice compared with controls (set to 100%). The asterisk indicates statistical significant change (P < 0.05). The cross indicates that the majority of mice do not survive beyond this time point. Each dot represents the mean value obtained from three to four mice. (B) FACS plots (top) and bar graph (bottom) showing the percentage of BrdU⁺ cells within the LSKCD135⁻ population in BM and spleen after 90 min and in BM after
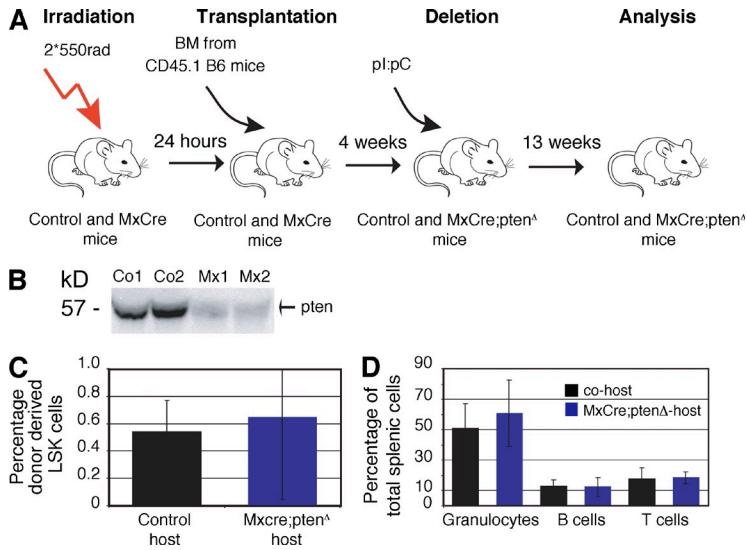
A

Irradiation	Transplantation	Deletion	Analysis
2*550rad	BM from CD45.1 B6 mice	pI:pC	

24 hours → 4 weeks → 13 weeks →

Control and MxCre mice → Control and MxCre mice → Control and MxCre;pten^Δ mice → Control and MxCre;pten^Δ mice

B

kD	Co1	Co2	Mx1	Mx2
57 -				← pten

C Percentage donor derived LSK cells — Control host / Mxcre;pten^Δ host

D Percentage of total splenic cells — Granulocytes, B cells, T cells (co-host ■; MxCre;ptenΔ-host ■)

Figure 5. Pten loss mobilizes HSCs in a hematopietic cell–autonomous manner. (A) Experimental setup used to generate reverse chimeras. (B) PTEN expression in BM stromal cells by Western blot. (C) Percentage of donor-derived wild-type LSK cells isolated from control and MxCre;pten^Δ hosts. black, co-host; blue, MxCre;pten^Δ host. P > 0.05. n = 3 MxCre;pten^Δ, n = 3 control mice. (D) Percentages of donor-derived wild-type mature granulocytes, B cells, and CD4 T cells in spleens isolated from control and MxCre;pten^Δ hosts. P > 0.05. n = 3 MxCre;pten^Δ, n = 3 control mice. Data are provided as mean ± SE.

any significant difference in cell cycle behavior or dormancy status between normal and *Pten*-deficient HSCs.

Pten^ΔScl and *Pten*^ΔMx HSCs are functional and retain basal Akt levels, but accumulate in the spleen

Our results suggest that the disappearance of *Pten*-deficient HSCs in the BM is not caused by increased HSC proliferation, followed by exhaustion. To search for an alternative explanation, we examined whether *Pten* mutant HSCs might have migrated from the BM to the spleen, which is known to massively increase in *Pten* mutant animals. Indeed, the total number of LSKCD34⁻CD135⁻ cells in the spleen dramatically increased in both models after loss of *Pten*, raising the possibility that HSCs are not physically lost but rather relocate to the spleen (Fig. 4 F). To answer this question, we first assessed whether *Pten*-deficient phenotypic HSCs are functional in both locations. Indeed, although the reconstitution activity of *Pten*-deficient splenocytes was dramatically increased compared with controls, *Pten*-deficient BM contained reduced

HSC activity (Fig. 4 G). To confirm these results, we performed limiting dilution experiments by transplanting into lethally irradiated recipients a limiting amount of control and mutant BM cells (0.4% of total BM) and splenocytes (1.6% of total splenocytes). As shown in Fig. 4 H, *Pten*-deficient BM contained a lower number of competitive repopulation units (CRUs) when compared with control BM. CRU numbers were, instead, increased in Pten-deficient spleen. This analysis suggests that the spatial distribution of HSCs is altered in *Pten*-deleted mice relative to control mice, whereas the absolute numbers of HSCs appear to be the same.

Assaying reconstitution of *Pten*-deficient BM beyond 9 wk is complicated by the fact that the BM already contains precancerous clones which progress after transplantation and thus are likely responsible for the observed sudden increase in chimerism. To circumvent this complication, 2,500 FACS-sorted LSK-HSCs from *Pten*^ΔMx and control mice were transplanted together with rescue BM. Interestingly, *Pten*-deficient HSCs showed the same multilineage reconstitution activity

18 h of BrdU labeling. P = 0.99, P = 0.19, and P = 0.75, respectively. (C) Percentage of BrdU LRCs within the LSKCD34⁻CD135⁻population. Mice were initially labeled for 10 d with BrdU, followed by simultaneous induction of SCL-CreERT with Tx and 70 d of a BrdU free chase period. P = 0.02. Each dot represents a single mouse. Horizontal bars indicate mean values. (D) Kaplan-Meyer curve showing the survival of *Pten*^ΔMx and *Pten*^ΔScl mice (15 d [Mx] or 21 d [Scl] after deletion) during weekly 5-FU administration. n = 7 *Pten*^ΔMx mice, n = 4 *Pten*^ΔScl mice, n = 4 of each control group. (E) Analysis of intracellular Ki67 expression in LSKCD135⁻ cells from BM (top, P = 0.43) and spleen (bottom, P = 0.81) of pten^ΔMx mice. (F) Kinetic analysis of the relative change of LSKCD34⁻CD135⁻ cells in the spleen of *Pten*^ΔMx and *Pten*^ΔScl mice compared with controls (set to 100%). The asterisk indicates statistically significant change (P < 0.05). The cross indicates that the majority of mice do not survive beyond this time point. Each dot represents the mean value obtained from three to four mice. (G) Bar graph showing CD45.2 donor contribution 5, 7, and 9 wk after transplantation of 0.4% of total BM and 1.6% of total splenocytes of control and *Pten*^ΔMx mice into CD45.1 hosts. n = 4 each group. (H) Limiting dilution analysis of BM cells (top) and splenocytes (bottom) of pten^ΔMx (KO) and control (wt) mice. Values represent reconstituted mice (chimerism > 0.5%) versus total mice transplanted. CRUs were calculated using the method of maximum likelihood. The number of mice per group is indicated. (I) Percentage of CD45.2 donor contribution 12 wk after transplantation of 2500 LSK cells of control and *Pten*^ΔMx mice into CD45.1 hosts. (J and K) Multilineage reconstitution after transplantation of 2500 BM (J) or splenic (K) LSK cells from pten^ΔMx mice. n = 2 controls, n = 3 mutants. (L) PCR analysis of DNA from FACS-sorted donor (CD45.2) splenocytes 12 wk after transplantation showing the absence of the *Pten*^flox but presence of the *Pten*Δ allele. (M–O) *Pten*, pAktTh308, pAktSer473, and pGSK3βSer9 levels in BM LSKCD135⁻CD34⁻ (top) or splenic LSK cells (bottom) of *Pten*^ΔMx and controls (pI-pC treated). A representative FACS plot (M) and the fold change in the expression levels (N and O) are shown. Three independent experiments, n = 6 for each group. BM: P = 0.01 *Pten*, P > 0.05 pAktTh308, pAktSer473, and pGSK3βSer9. Spleen: P = 0.04 *Pten*, P > 0.05 pAktTh308, pAktSer473, and pGSK3βSer9. Unless otherwise indicated, the data presented in this figure refer to at least three independent experiments using at least three mice per group. Data are provided as mean ± SE.
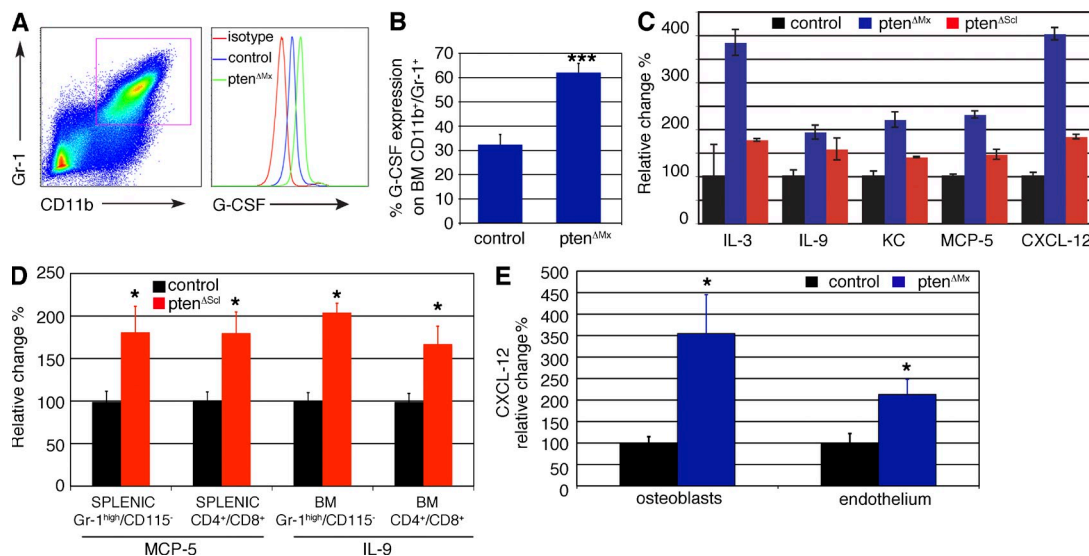
Figure 6.   Increased level of mobilizing cytokines in pten$^{\Delta Mx}$ and pten$^{\Delta Scl}$ mice. (A and B) FACS plot (A) and histogram showing GCSF expression in BM CD11b$^+$Gr-1$^+$ cells of control and *Pten*$^{\Delta Mx}$ mice. Two independent experiments were done for controls (*n* = 7) and mutants (*n* = 8; *** indicates statistically significant change, P = 0.0008). (C) Cytokine array screen showing serum levels of indicated cytokines 15 d (*Pten*$^{\Delta Mx}$) or 28 d (*Pten*$^{\Delta Scl}$) after deletion. This screen has been performed once with *n* = 2 per group. (D) MCP-5 and IL-9 levels in splenic Gr-1^{high}/CD115$^-$ and CD4$^+$CD8$^+$ cells or BM CD11b$^+$Gr-1$^+$ and CD4$^+$CD8$^+$ cells of *Pten*$^{\Delta Scl}$ mice and control counterparts. Data are shown as fold change as compared with control levels. P = 0.01, MCP-5 in Gr-1^{high}/CD115$^+$ cells. P = 0.007, MCP-5 in CD4$^+$CD8$^+$ cells. P = 0.03, IL-9 in BM CD4$^+$CD8$^+$ cells. P = 0.04, IL-9 in BM CD11b$^+$Gr-1$^+$ cells. Three independent experiments were performed, *n* = 11 controls and *n* = 6 mutants. (E) CXCL-12 levels observed in osteoblasts (CD45$^-$CD31$^-$Ter119$^-$CD51$^+$Sca-1$^-$ cells) and endothelial cells (CD45$^-$Ter119$^-$CD31$^+$) of *Pten*$^{\Delta Mx}$ mice and controls. Data are shown as fold change as compared with control levels. Two independent experiments (5 controls and 10 mutants) were performed. P < 0.01, osteoblasts, P < 0.05 endothelial cells. Data are provided as mean ± SE. Unless otherwise indicated, * indicates statistically significant change with P < 0.05.

(with the notable exception of B cells) after 3 mo as their normal counterparts (Fig. 4, I–L), demonstrating that *Pten*-deficient BM and splenic HSCs have myelo/lymphoid reconstitution potential. In agreement with their normal function, BM LSKCD34$^-$ and splenic LSK cells of *Pten*$^{\Delta Mx}$ and *Pten*$^{\Delta Scl}$ mice did not show an increase in the levels of P-AKTthr308, P-AKTser473, or P-GSK3βser9, despite *Pten* being deleted (Fig. 4, M–O; and not depicted). To exclude that these results could be due to a poor sensitivity of the detergent-based assay used to detect phospho-antigens, we further evaluated AKT levels by using an alternative paraformaldehyde/acetone method (Krutzik et al., 2011). However, with this method, AKT activation was also exclusively found in *Pten*-deficient myeloid cells and not in HSCs (unpublished data). Surprisingly, these data indicate that PI3K-Akt signaling is not significantly up-regulated in *Pten*-deficient HSCs. Collectively, these results suggest that *Pten*-deficient HSCs are functional and retain basal levels, but not significantly increased P-AKT levels, and are predominantly localized in the spleen rather than in the BM. To further address whether *Pten* deletion in the stromal compartment contributes to HSCs relocalization to the spleen, we performed reverse chimeras experiments. Wild-type cells were transplanted into lethally irradiated *Pten*^{flox2} or MxCre;*Pten*^{flox2} hosts, and after hematopoietic reconstitution, *Pten* deletion was induced by pI-pC (Fig. 5 A). Although *Pten* was efficiently deleted in BM stroma (Fig. 5 B), *Pten*$^{\Delta Mx}$ and control recipients presented a similar number of donor-derived LSK cells in their spleens (Fig. 5 C). Moreover,

no changes in the distribution of donor-derived mature splenic cells were observed in *Pten*$^{\Delta Mx}$ recipients (Fig. 5 D). These data show that *Pten* loss–induced relocalization of HSCs to the spleen is due to a hematopoietic cell autonomous mechanism.

Pten deletion increases expression of mobilizing cytokines
Accumulation of normal HSCs in the spleen is observed after BM injury and establishment of extramedullary hematopoiesis, or in response to high levels of mobilizing cytokines such as G-CSF. Therefore, we examined whether the level of this cytokine was increased after *Pten* deletion. As shown in Fig. 6 (A and B), *Pten* mutant CD11b$^+$Gr1$^+$ BM cells produced significantly higher G-CSF levels as compared with their control counterparts (Fig. 6, A and B; and not depicted). To examine whether other cytokines were increased in *Pten*-deficient serum, a cytokine antibody array screen was used to simultaneously study the expression of 62 cytokines. This global analysis revealed that, in addition to G-CSF, levels of both CXCL12, and the mouse analogue of human IL-8, known as keratinocyte-derived chemokine (KC), were elevated (Fig. 6 C). The results obtained in this screen were then validated by flow cytometry. As shown in Fig. 6 D, MCP-5 was significantly increased in mutant splenic Gr-1^{high}CD115$^-$ and CD4$^+$/CD8$^+$ cells. In addition, a threefold up-regulation of IL-9 occurred in mutant BM myeloid cells and lymphoid cells (Fig. 6 D) and *Pten*-deficient osteoblasts and endothelial cells produced higher levels of CXCL12 (Fig. 6 E). In summary,
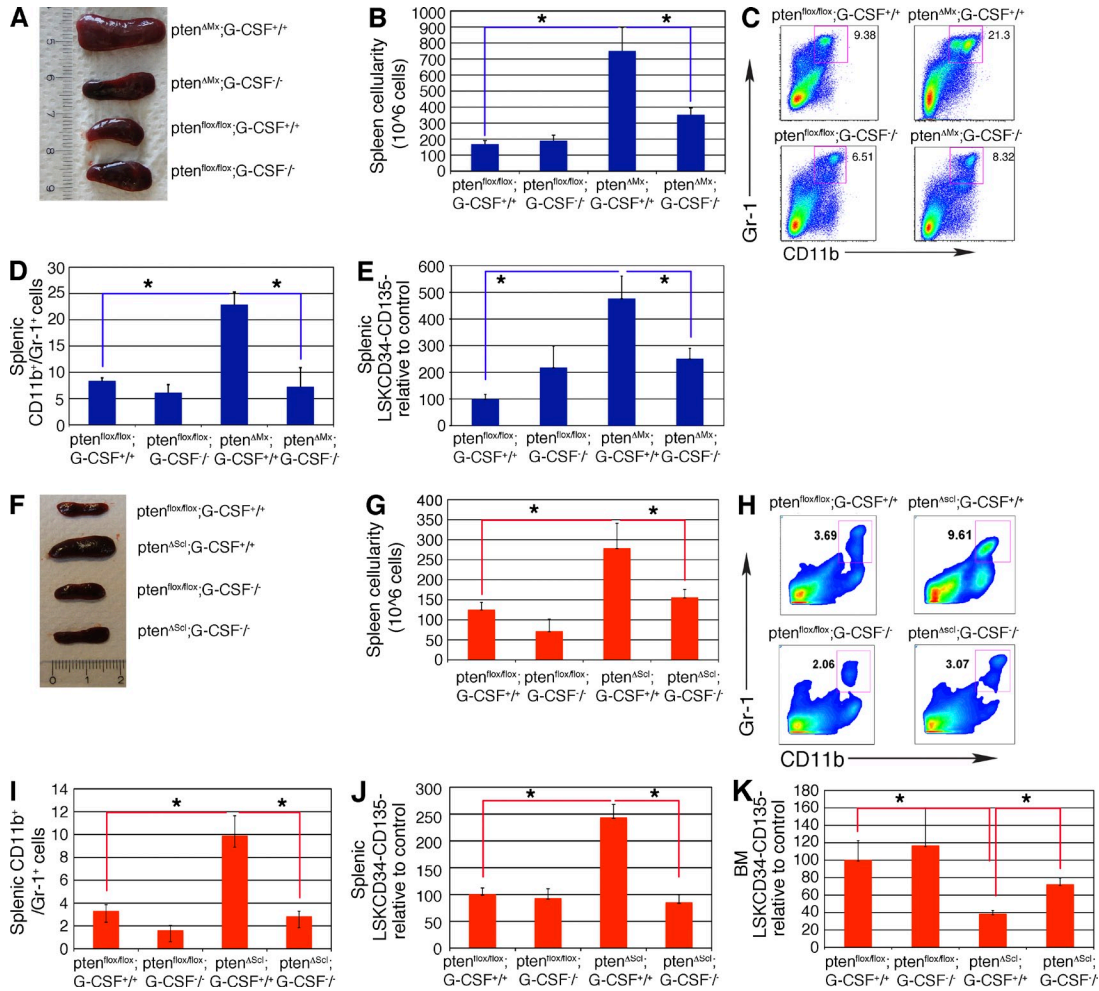
Figure 7. In the absence of G-CSF, the Pten mutant phenotype is rescued. (A) Spleens of $Pten^{fl/fl}$, $Pten^{fl/fl}$;G-CSF$^{-/-}$, $Pten^{\Delta Mx}$;G-CSF$^{-/-}$, or $Pten^{\Delta Mx}$;G-CSF$^{+/+}$ 15 d after deletion. (B) Splenic cellularity of $Pten^{fl/fl}$, $Pten^{fl/fl}$;G-CSF$^{-/-}$, $Pten^{\Delta Mx}$;G-CSF$^{-/-}$, or $Pten^{\Delta Mx}$;G-CSF$^{+/+}$ 15 d after deletion. $Pten^{fl/fl}$ versus $Pten^{\Delta Mx}$;G-CSF$^{+/+}$, P = 0.02. $Pten^{\Delta Mx}$;G-CSF$^{+/+}$ versus $Pten^{\Delta Mx}$;G-CSF$^{-/-}$, P = 0.04. $Pten^{fl/fl}$ versus $Pten^{fl/fl}$ G-CSF$^{-/-}$, P = 0.36. (B–E) Four independent experiments, n = 7 each group. (C and D) Percentages of CD11b$^+$Gr-1$^+$ cells in the spleens of $Pten^{fl/fl}$, $Pten^{fl/fl}$;G-CSF$^{-/-}$, $Pten^{\Delta Mx}$;G-CSF$^{-/-}$, or $Pten^{\Delta Mx}$;G-CSF$^{+/+}$ 15 d after deletion. $Pten^{fl/fl}$ versus $Pten^{\Delta Mx}$;G-CSF$^{+/+}$, P = 0.01. $Pten^{\Delta Mx}$;G-CSF$^{+/+}$ versus $Pten^{\Delta Mx}$;G-CSF$^{-/-}$, P = 0.01. $Pten^{fl/fl}$ versus $Pten^{fl/fl}$ G-CSF$^{-/-}$, P = 0.29. (E) Relative changes in splenic LSKCD34$^-$CD135$^-$ levels. $Pten^{fl/fl}$ versus $Pten^{\Delta Mx}$;G-CSF$^{+/+}$, P = 0.04. $Pten^{\Delta Mx}$;G-CSF$^{+/+}$ versus $Pten^{\Delta Mx}$;G-CSF$^{-/-}$, P = 0.04. $Pten^{fl/fl}$ versus $Pten^{fl/fl}$ G-CSF$^{-/-}$, P = 0.07. (F) Spleens of $Pten^{\Delta Mx}$;G-CSF$^{-/-}$ or $Pten^{\Delta Scl}$;G-CSF$^{+/+}$ mice or their control counterpart $Pten^{fl/fl}$ and or $Pten^{fl/fl}$;G-CSF$^{-/-}$ after 28 d of Tx diet. (G) Splenic cellularity of $Pten^{\Delta Mx}$;G-CSF$^{-/-}$ or $Pten^{\Delta Scl}$;G-CSF$^{+/+}$ mice or their control counterpart $Pten^{fl/fl}$ and or $Pten^{fl/fl}$;G-CSF$^{-/-}$ after 28 d of Tx diet. $Pten^{fl/fl}$ versus $Pten^{\Delta Scl}$;G-CSF$^{+/+}$, P = 0.026. $Pten^{\Delta Scl}$;G-CSF$^{+/+}$ versus $Pten^{\Delta Scl}$;G-CSF$^{-/-}$, P = 0.047. Five independent experiments, n = 10 each group. (H and I) CD11b$^+$Gr-1$^+$ cells in the spleens of $Pten^{\Delta Scl}$;G-CSF$^{-/-}$, $Pten^{\Delta Scl}$;G-CSF$^{+/+}$, $Pten^{fl/fl}$, or $Pten^{fl/fl}$;G-CSF$^{-/-}$ mice which were fed with Tx for 28 d. A representative FACS plot and a histogram are shown in E and G, respectively. $Pten^{fl/fl}$ versus $Pten^{\Delta Scl}$;G-CSF$^{+/+}$, P = 0.029. $Pten^{\Delta Scl}$;G-CSF$^{+/+}$ versus $Pten^{\Delta Scl}$;G-CSF$^{-/-}$, P = 0.002. Three independent experiments are shown, n = 7 each group (H and K). (J) Relative changes in the levels of LSKCD34$^-$CD135$^-$ in the BM and spleen of $Pten^{\Delta Scl}$;G-CSF$^{-/-}$, $Pten^{\Delta Scl}$;G-CSF$^{+/+}$, $Pten^{fl/fl}$, or $Pten^{fl/fl}$;G-CSF$^{-/-}$ mice. $Pten^{fl/fl}$ versus $Pten^{\Delta Scl}$;G-CSF$^{+/+}$, P = 0.036. $Pten^{\Delta Scl}$;G-CSF$^{+/+}$ versus $Pten^{\Delta Scl}$;G-CSF$^{-/-}$, P = 0.042. (K) Relative changes in the levels of LSKCD34$^-$CD135$^-$ in the BM and spleen of $Pten^{\Delta Scl}$;G-CSF$^{-/-}$, $Pten^{\Delta Scl}$;G-CSF$^{+/+}$, $Pten^{fl/fl}$, or $Pten^{fl/fl}$;G-CSF$^{-/-}$ mice. $Pten^{fl/fl}$ versus $Pten^{\Delta Scl}$;G-CSF$^{+/+}$, P = 0.037. $Pten^{\Delta Scl}$;G-CSF$^{+/+}$ versus $Pten^{\Delta Scl}$;G-CSF$^{-/-}$, P = 0.16. Data are provided as mean ± SE. Unless otherwise indicated, * indicates statistically significant change with P < 0.05.

the up-regulation of cytokine production, including G-CSF, provides a mechanistic explanation for the observed mobilization of *Pten*-deficient HSCs from the BM to the spleen.

Genetic elimination of G-CSF rescues *Pten* loss–induced phenotypes

Next, we examined whether the genetic lack of G-CSF could rescue the phenotype observed in $Pten^{\Delta Mx}$ and $Pten^{\Delta Scl}$ mice.

$Pten^{\Delta Mx}$;$G\text{-}CSF^{-/-}$ double-mutant mice did not develop splenomegaly (Fig. 7, A and B), nor did they massively increase the number of splenic CD11b$^+$Gr-1$^+$ cells (Fig. 7, C and D). Importantly, $Pten^{\Delta Mx}$;$G\text{-}CSF^{-/-}$ mice did not accumulate LSKCD34$^-$CD135$^-$ cells in their spleens (Fig. 7 E). Similarly, $Pten^{\Delta Scl}$;$G\text{-}CSF^{-/-}$ mice showed no significant increase in spleen size when compared with control animals (Fig. 7, F and G). Moreover, $Pten^{\Delta Scl}$;$G\text{-}CSF^{-/-}$ animals did

not accumulate CD11b$^+$Gr-1$^+$ cells in their spleen as observed in Pten$^{\Delta Scl}$;G-CSF$^{+/+}$ mice (Fig. 7, H and I). As expected, Pten$^{fl/fl}$;G-CSF$^{-/-}$ mice only demonstrated a modest nonsignificant decrease in the number of splenic immature myeloid cells (Fig. 7, H and I). Additionally, the significant accumulation of LSKCD34$^-$CD135$^-$ cells observed in the spleen of Pten$^{\Delta Scl}$;G-CSF$^{+/+}$ mice did not occur in the absence of G-CSF (Fig. 7 J). Consistent with these observations, Pten$^{\Delta Scl}$; G-CSF$^{-/-}$ mice showed a moderate increase in the numbers of BM LSKCD34$^-$CD135$^-$ cells when compared with Pten$^{\Delta Scl}$; G-CSF$^{+/+}$ animals (Fig. 7 K). Importantly, Pten$^{\Delta Scl}$;G-CSF$^{-/-}$ mice did not significantly differ in the numbers of splenic or BM HSCs compared with controls (Fig. 7, J and K).

In summary, our data suggest that loss of Pten promotes HSC mobilization to the spleen, which is caused by the production of G-CSF by mutant BM myeloid cells. Thus, HSC mobilization in mutants is not a cell-autonomous effect caused by the lack of Pten in HSCs but rather a consequence to the loss of Pten in myeloid and stromal cells. This, in turn, induces the secretion of cytokines that feeds back to HSCs in their BM niche leading to their mobilization to the spleen.

DISCUSSION

In this study, we generated a new conditional SclCre–mediated Pten KO model, which enabled us to provide new mechanistic insights into the role of Pten in the hematopoietic stem and progenitor cells. Particularly, we show that Pten deletion induces production of G-CSF in myeloid cells, which subsequently leads to HSC mobilization to the spleen, followed by development of MPD and leukemia.

Although some of our data are consistent with previous studies showing that Pten deletion promotes MPD, leukemia development, and loss of HSCs in the BM, our data challenge the suggested mechanism in which Pten is put forward as an important regulator of HSC proliferation and self-renewal. (Chen et al., 2006; Yilmaz et al., 2006; Lee et al., 2010). Instead, our results suggest an indirect role for Pten in HSCs mobilization. Pten mutant mice in our hands have a normal number of quiescent and dormant HSCs, and a normal stress response after 5-FU induced myeloid ablation. Consistently, the expression profiles of control and Pten–deficient HSCs have revealed a strikingly overlapping pattern with only very few differentially expressed genes after Pten deletion (unpublished data). In agreement with these data, transplantation studies showed that Pten–deficient HSCs can generate all hematopoietic lineages (except mature B cells) and are fully functional. Strikingly, no activation of AKT signaling was observed on BM LSKCD34$^-$ cells after Pten loss. Collectively, our ex vivo and in vivo studies revealed neither a significant role for PTEN in the control of the balance between HSC quiescence and self-renewal nor a critical role for HSC function, as was previously suggested (Yilmaz et al., 2006).

As an alternative mechanism for the observed loss of Pten–deficient BM HSCs, our data provide strong evidence that upon Pten deletion, functional HSCs are mobilized from the BM to the spleen. This is mediated by expression of several

cytokines by mutant myeloid cells, which are known to mobilize HSCs. These include KC, the mouse homologue of the CXC chemokine IL-8, a chemoattractant and activator of neutrophils previously shown to rapidly induce mobilization of HSCs in mice and primates (Laterveer et al., 1995). In addition, after Pten deletion, CXCL12, a well characterized chemoattractant for HSCs and a key mediator of HSC trafficking (Lapidot and Petit, 2002; Nervi et al., 2006; Tesio et al., 2011), is up-regulated. Finally, and most importantly, mutant myeloid cells significantly up-regulate G-CSF, the most common mobilizing cytokine routinely used for harvesting human HSC from donors in clinical settings (Nervi et al., 2006). The exact molecular mechanisms that up-regulate G-CSF expression in myeloid cells after Pten loss remains to be explored. However, it may be mediated by the KC/IL-8 receptor Cxcr2, which has been previously implicated in G-CSF regulation (Mei et al., 2012).

The role of G-CSF is critical, as Pten mutant cells lacking the G-CSF gene fail to significantly mobilize HSCs to the spleen. Nevertheless, G-CSF may have other functions that contribute to the phenotype. Moreover, the additional mobilizing cytokines increased upon PTEN deletion may also contribute to the egress of mutant HSCs. This phenomenon, moreover, is induced by mutant BM immature myeloid cells and does not appear to be a cell-intrinsic phenomenon of HSCs. Indeed, despite Pten being efficiently deleted in HSCs, no activation of the PI3K–AKT pathway could be detected. In contrast, mutant CD11b$^+$Gr-1$^+$ cells displayed activated Akt signaling in response to Pten loss. Thus, our results indicate that loss of Pten in BM myeloid cells is the driving force leading to G-CSF production and HSC mobilization to the spleen. In agreement with these data, recent studies revealed the crucial role of BM myeloid cells such as monocytes and macrophages in driving HSC egress from their niches (Winkler et al., 2010; Chow et al., 2011). Interestingly G-CSF signaling in BM monocytes was shown to be sufficient to induce HSC mobilization (Christopher et al., 2011); however, the molecular mechanisms underlying these processes remain mostly uncertain.

Because AKT signaling is not altered in Pten–deficient HSCs, other phosphatases might be operative in HSCs. Another negative regulator of the PI3K pathway, SHIP, is a potential candidate, as it was shown to cooperate with Pten in B cell lymphoma (Miletic et al., 2010). Additionally the serine/threonine phosphatase PP2A negatively regulates P-AKT in human CD34$^+$ progenitor cells, contributing to their motility (Basu et al., 2007). Interestingly, our results demonstrate that HSCs and myeloid cells show a different degree of AKT activation in response to Pten deletion. Mammalian cells express three isoforms, AKT1, AKT2, and AKT3, with the first two being expressed in hematopoietic cells. Functional differences between these two isoforms have been shown, and AKT1 and AKT2 deletion in Pten heterozygous mice have different effects on tumorigenesis (Chen et al., 2006; Xu et al., 2012). Importantly, the amplitude of AKT inactivation by PHLPP phosphatases largely depends on the isoform type (Brognard et al., 2007). Thus, a differential expression and/or activity of the two

AKT isoforms in myeloid and HSCs might explain why the two cell types show a different response to *Pten* deletion.

Several lines of evidence indicate that splenomegaly and MPD development are, at least partially, a secondary effect of *Pten* deficiency in BM myeloid cells. First, the production of G-CSF by mutant BM CD11b+Gr-1+ cells is crucial for the development of splenomegaly and MPD, as both phenomena were abolished in mice lacking G-CSF. Second, *Pten*-deficient myeloid cells do show overactive AKT signaling, which is crucial in driving MPD development (Kharas et al., 2010). The role of AKT in HSC self-renewal is controversial, as its constitutive activation was shown to deplete HSCs (Kharas et al., 2010), whereas fetal liver HSCs lacking AKT were unable to reconstitute long-term hematopoiesis (Juntilla et al., 2010). Our data, showing that HSC self-renewal is maintained in the presence of a physiological level of active AKT, indicate that a fine-tuned modulation of AKT activation guarantees HSC maintenance, whereas too low or too high levels are detrimental for HSC function. In any case, PTEN does not seem to be a major regulator for AKT activity in HSCs in vivo.

The discrepancies observed between this and previous studies, with respect to HSC proliferation and AKT activation, might be due to the different genetic background used. Previous studies used mice on a clean C57BL/6 inbred background; in contrast, our data are obtained with mice on a mixed genetic background. These data may indicate that the observed effects on a C57BL/6 background are strain specific and our model might therefore better reflect the genetic complexity observed in clinical settings. This difference might be crucial, as several aspects of HSC function show genetically determined variation and HSC cycling activity, as well as HSC pool size being controlled at a genetic level (Van Zant et al., 1983; de Haan and Van Zant, 1997). Similarly, strain-dependent variations affect responsiveness of primitive progenitor cells to cytokines such as SCF, Flt3 ligand, and TGF-β (Henckaerts et al., 2002, 2004; Avagyan et al., 2008). Intriguingly, the mobilization response to G-CSF is also affected by genetic variation (Hasegawa et al., 2000). Moreover, tumor development in *Pten*-deficient mice has been demonstrated to be highly dependent on genetic background (Freeman et al., 2006; Svensson et al., 2011).

Interestingly, although in the absence of G-CSF *Pten* mutant mice do not develop splenomegaly or accumulate HSCs in their spleens, G-CSF absence did not rescue T-ALL development (unpublished data). Additional mechanisms, such as activation of Notch signaling, might be involved in this phenomenon. Mutations in NOTCH1 are the most recurrent genetic lesions in T-ALL, and a cross talk between PTEN and NOTCH1 signaling in regulating T-ALL development has been reported (Palomero et al., 2007). Furthermore, a recent study has suggested that PTEN down-regulation contributes to the activation of the oncogene c-Myc, providing another mechanism for the promotion of T-ALL in the absence of PTEN (Bonnet et al., 2011).

Collectively, our data provide a novel and important mechanism for HSCs mobilization and MPD initiation,

indicating that PTEN is dispensable for HSCs but critical for proliferation and cytokine production of myeloid progenitors. In conclusion, our data show that in response to *Pten* loss, BM Gr-1+CD11b+ cells hyper-activate AKT signaling and up-regulate G-CSF, which promotes HSC accumulation in the spleen, splenomegaly, and MPD development. The increased G-CSF levels are further supported by elevated CXCL-12 production by mutant stromal and endothelial cells to promote mobilization of HSCs from the BM to the spleen. Importantly, mobilized *Pten*-deficient splenic HSCs are functional, as they maintain their self-renewal activity and do not show increased AKT activation. Inhibition of AKT signaling by one of the various inhibitors in leukemia patients would therefore lead to the return of mobilized HSCs to the BM with little if any direct functional effects on the HSCs themselves.

MATERIALS AND METHODS

Mice. All mice were maintained in the ISREC and in the DKFZ animal facility under specific pathogen–free (SPF) conditions and housed in individually ventilated cages (HIVC). Animal procedures were performed according to protocols approved by the Swiss Bundesamt für Veterinärwesen no. 1728 and by the German authorities no. G-22/09. *Pten*flox/flox (control) mice (The Jackson Laboratory) were purchased as in Groszer et al. (2001) and crossed with the MxCre transgenic mice (Kühn et al., 1995) to obtain MxCre;*Pten*flox/flox (mutant) mice on a mixed genetic background (∼50% C57BL/6, rest 129SV, FVB/N). IFN-α–induced deletion was induced by five i.p. injections of 10 mg/kg polyI-polyC (poly-IC; InvivoGen) every 2 d as previously described (Wilson et al., 2004). For the LRC assay, mice were BrdU labeled for 10 d using 0.8 mg/ml BrdU water (glucose), followed by a 70-d chase. 5-FU studies were performed using weekly i.p. injections of 150 mg/kg 5-Fluorouracil (Sigma-Aldrich). Unless otherwise stated, all control mice were littermates of analyzed mutant mice and were all treated with pI-pC. *Pten*flox/flox (control) mice were crossed with the SCL-CreER[T] transgenic mice (Göthert et al., 2005) to obtain SCL-CreER[T];*Pten*flox/flox (mutant) mice on a mixed genetic background (63% C57BL/6; 47% 129SVJ and CBA/J). Recombination was achieved by Tx diet (1 g/kg food; Sigma-Aldrich) for 20 d. G-CSF−/− mice were provided by G.J. Lieschte (Australian Regenerative Medicine Institute, Victoria, Australia).

Generation and analysis of chimeras. B6.SJL-Ptprca-Pep3b-/BoyJ donor mice (CD45.1; The Jackson Laboratory) were purchased and maintained in the ISREC animal facility. To generate HSC chimeras, transplantation was performed using 2,500 FACS-sorted LSK-HSCs from each donor mouse, along with 2×10^6 CD45.1 rescue BM cells, which were i.v. transferred into two CD45.1+ lethally irradiated (2×550 rad) recipient mice, which were been pretreated (48 h before) with anti–NK1.1 mAb. For limiting dilution transplants, the indicated dilutions of BM and SP CD45.2 cells from experimental mice were transferred i.v., along with 1.5×10^6 Sca1-depleted CD45.1 BM into lethally irradiated CD45.1 recipients. To address the leukemic potential of Pten-deficient cells, control and mutant cells were transplanted into sublethally irradiated NOD/SCID recipients. All chimeric mice were maintained on antibiotics containing water (Bactrim; Roche) for 3 wk after irradiation, and long-term reconstitution of peripheral blood, BM, and spleen was analyzed 1–3 mo later. CRU frequencies were calculated using Poisson statistics and the method of maximum likelihood from the proportions of animals that were not reconstituted (<0.5% chimerism; Szilvassy et al., 1990). To generate reverse chimeras, wild-type CD45.1 BM cells were transplanted into lethally irradiated *Pten*flox2 or MxCre;*Pten*flox2 mice (CD45.2). After 4 wk, the hematopoietic reconstitution was analyzed and *Pten* deletion was induced by polyI-C. 13 wk later, the chimerism was analyzed by flow cytometry. Western blotting: 10^6 BM or SP cells were lysed in 100 µl Laemmli-buffer for 5 min at 95° for degradation, and an insulin syringe was used for homogenization. Ms*Pten* (Cell Signaling Technology), msGAPDH

(EMD Millipore), and antibodies, followed by anti–mouse-HRP (Promega) and the ECL WB detection kit (GE Healthcare), were used for blot development.

Isolation of BM, spleen, and stromal cells. To collect BM cells, mouse legs were dissected and flesh removed, bones were crushed using a mortar and pestle, and cell suspensions were filtered before further use. Mouse spleens were isolated and crushed using the bottom of a syringe punch and filtered to obtain cell suspensions. Blood cells were collected from tail vein bleedings into tubes containing 10,0000 U/ml heparin (Sigma-Aldrich) and peripheral blood lymphocyte were isolated using a histopaque gradient (1,900 rpm, 8 min, no brake; Sigma-Aldrich). To isolate HSCs, lineage magnetic depletion was performed to enrich for lineage-negative cells. Therefore, BM cells were incubated with lineage antibodies (CD4, CD8, CD11b, Gr1, B220, and Ter119) and lineage-positive cells were removed using sheep anti–rat IgG-coated M450 Dynabeads (Invitrogen). Lineage-negative cells were stained for hematopoietic subsets, and LSK-HSCs were sorted using a FACS-Aria (BD). Stromal cells were obtained by three subsequent digestions of the leg bones. In brief, the bones were first digested with a solution containing Trypsin 0.1% Collagenase P and DNase (20 min at 37°C). Bones were then washed and crushed. The remaining bone fragments were then incubated with a second solution containing trypsin 0.1% and DNase (20 min at 37°). After being washed, bone fragments underwent a third digestion containing collagenase P, dispase, Hepes, and CaCl$_2$ (1 h at 37°C). The cells present in the supernatant were isolated using a histopaque gradient.

Flow cytometry and cell cycle analysis. Cell cycle analysis on HSCs was performed using a cell surface staining in combination with BrdU or Ki67 antibodies. For BrdU analysis, mice were injected i.p. with 7.2 mg/kg BrdU (Sigma-Aldrich) before analysis. Mice were sacrificed and BM and SP cells were isolated. Lineage bead depletion was performed to enrich for lineage-negative cells. Lineage–negative cells were stained for hematopoietic subsets using lineage antibodies (see below) CD117, Sca1, and CD135. For BrdU staining, a commercial kit (BD) was used. The same BrdU kit was used to fix and permeabilize the cells and was followed by anti–human Ki67 (BD) antibody incubation overnight. For flow cytometric analysis, the four-color FACSCalibur (BD) equipped with a 488 and 635 nm laser, the six-color FACSCanto (BD) equipped with a 488 and a 633 nm laser, or the LSR (BD) flow cytometer equipped with a 488 nm and UV (305 nm) laser were used. Stromal cells were stained with CD45, Ter119, CD31, CD51, and Sca-1 antibodies (eBioscience). Osteoblasts were defined as CD45⁻Ter119⁻CD31⁻CD51⁺Sca-1⁻ and endothelial cells as CD45⁻Ter119⁻CD31⁺ cells. The intracellular expression of G-CSF, P-AKTser473, P-AKTth308, and pGSK3βser9 was detected by flow cytometry on BM cells, which were stained for extracellular surface markers and then fixed and permeabilized using the Cytofix/Cytoperm kit according to the manufacturer's instructions (BD). P-AKT-ser478 levels were additionally evaluated using an alternative methanol-based permeabilization protocol (Krutzik et al., 2011). Statistical analysis for all flow cytometric studies was performed using a two-tailed Student's t test.

Immunohistochemistry. All histological samples were collected and fixed in 10% neutral buffered formalin solution (HT50 1–2; Sigma-Aldrich) for 2-4 h in a cold room on a rotor. For bones, an additional decalcification step in 0.4 M EDTA, pH 7.2, for 4–6 d at 4°C was performed on a rotor. For immunohisto-chemistry, slides were pretreated with peroxidase blocking buffer (120 mM Na$_2$HPO$_4$, 43 mM citric acid, 30 mM NaN$_3$, and 0.2% H$_2$O$_2$, pH 5.8) prior to antigen retrieval (20 min at 70°C, 10 mM citrate buffer, pH 6.0) and then sections were incubated with a rabbit polyclonal *Pten* antibody (Neomarkers, 1:200; LAB VISION), followed by an anti–rabbit HRP (Dako). DAB (Sigma-Aldrich) was used to reveal staining, and Mayers Hematoxylin (Sigma-Aldrich) was used to counterstain the nucleus. Light microscopic analysis was performed using an Axio Scope equipped with a Progress C10ᵖˡᵘˢ camera (Carl Zeiss).

ELISA and cytokine array. Cytokine levels in the serum were quantified using the RayBio Mouse Cytokine Array III kit (Hoelzel Biotech) according to the manufacturer's protocol. The cytokine levels were calculated by measuring the normalized intensity of each spot, using AIDA Image Analyzer (v.4.06) software.

Antibodies. Gr-1 (Ly-6G, RB6-8C5)-FITC, -biotin, and -Alexa Fluor 647; Ter 119-FITC and –biotin; B220 (RA3-6B2)-FITC and -biotin; CD11b-FITC and -biotin; CD4 (clone GK1.5)-FITC and -biotin; CD8α (53.6.7)-FITC and -biotin; TCR-β (H57)–FITC; CD161 (NK1.1, PK136)-FITC and -biotin; CD45.1 (A20.1)-FITC, -biotin, -PE, or -Alexa Fluor 647; CD45.2 (ALI-4A2)-FITC, -biotin, -PE, or -Alexa Fluor 647; and TCR-γδ (GL3)–FITC and –Alexa Fluor 647 were purified and conjugated in this laboratory according to standard protocols. CD34 (RAM34)-FITC; CD135 (A2F10)-PE; CD117 (2B8)-PE and –PE-Cy5; Sca1 (D7)-APC and -biotin; CD43 (S7)-FITC, –BP1 (FG35.4)-biotin, and –IgM (11/41)-PE were all purchased from eBioscience. CD41 (MWReg30)–FITC was purchased from BD. Primary antibody anti–G-CSF was from Santa Cruz Biotechnology, Inc., and anti-pAKTthr308, -pAKTser473, and -pGSK3βser9 were from Cell Signaling Technology. Anti-CXCL12 antibodies were purchased from R&D Systems, anti–MCP-5-PE from Bioss, and IL-9–PE from BioLegend.

Statistical analysis. Significance levels of data were determined by Student's t test for the differences in mean values.

REFERENCES

Arai, F., A. Hirao, M. Ohmura, H. Sato, S. Matsuoka, K. Takubo, K. Ito, G.Y. Koh, and T. Suda. 2004. Tie2/angiopoietin-1 signaling regulates hematopoietic stem cell quiescence in the bone marrow niche. *Cell*. 118:149–161. http://dx.doi.org/10.1016/j.cell.2004.07.004

Avagyan, S., L. Glouchkova, J. Choi, and H.W. Snoeck. 2008. A quantitative trait locus on chromosome 4 affects cycling of hematopoietic stem and progenitor cells through regulation of TGF-beta 2 responsiveness. *J. Immunol*. 181:5904–5911.

Baccelli, I., and A. Trumpp. 2012. The evolving concept of cancer and metastasis stem cells. *J. Cell Biol*. 198:281–293. http://dx.doi.org/10.1083/jcb.201202014

Baldridge, M.T., K.Y. King, N.C. Boles, D.C. Weksberg, and M.A. Goodell. 2010. Quiescent haematopoietic stem cells are activated by IFN-gamma in response to chronic infection. *Nature*. 465:793–797. http://dx.doi.org/10.1038/nature09135

Basu, S., N.T. Ray, S.J. Atkinson, and H.E. Broxmeyer. 2007. Protein phosphatase 2A plays an important role in stromal cell-derived factor-1/CXC chemokine ligand 12-mediated migration and adhesion of CD34+ cells. *J. Immunol*. 179:3075–3085.

Bonnet, M., M. Loosveld, B. Montpellier, J.M. Navarro, C. Quilichini, C. Picard, J. Di Cristofaro, C. Bagnis, C. Fossat, L. Hernandez, et al. 2011. Posttranscriptional deregulation of MYC via PTEN constitutes a major alternative pathway of MYC activation in T-cell acute lymphoblastic leukemia. *Blood*. 117:6650–6659. http://dx.doi.org/10.1182/blood-2011-02-336842

Brognard, J., E. Sierecki, T. Gao, and A.C. Newton. 2007. PHLPP and a second isoform, PHLPP2, differentially attenuate the amplitude of Akt signaling by regulating distinct Akt isoforms. *Mol. Cell.* 25:917–931. http://dx.doi.org/10.1016/j.molcel.2007.02.017

Chen, M.L., P.Z. Xu, X.D. Peng, W.S. Chen, G. Guzman, X. Yang, A. Di Cristofano, P.P. Pandolfi, and N. Hay. 2006. The deficiency of Akt1 is sufficient to suppress tumor development in Pten+/- mice. *Genes Dev.* 20: 1569–1574. http://dx.doi.org/10.1101/gad.1395006

Chow, A., D. Lucas, A. Hidalgo, S. Méndez-Ferrer, D. Hashimoto, C. Scheiermann, M. Battista, M. Leboeuf, C. Prophete, N. van Rooijen, et al. 2011. Bone marrow CD169+ macrophages promote the retention of hematopoietic stem and progenitor cells in the mesenchymal stem cell niche. *J. Exp. Med.* 208:261–271. http://dx.doi.org/10.1084/jem.20101688

Christopher, M.J., M. Rao, F. Liu, J.R. Woloszynek, and D.C. Link. 2011. Expression of the G-CSF receptor in monocytic cells is sufficient to mediate hematopoietic progenitor mobilization by G-CSF in mice. *J. Exp. Med.* 208:251–260. http://dx.doi.org/10.1084/jem.20101700

Cross, D.A., D.R. Alessi, P. Cohen, M. Andjelkovich, and B.A. Hemmings. 1995. Inhibition of glycogen synthase kinase-3 by insulin mediated by protein kinase B. *Nature.* 378:785–789. http://dx.doi.org/10.1038/378785a0

de Haan, G., and G. Van Zant. 1997. Intrinsic and extrinsic control of hemopoietic stem cell numbers: mapping of a stem cell gene. *J. Exp. Med.* 186:529–536. http://dx.doi.org/10.1084/jem.186.4.529

Ding, L., T.L. Saunders, G. Enikolopov, and S.J. Morrison. 2012. Endothelial and perivascular cells maintain haematopoietic stem cells. *Nature.* 481:457–462. http://dx.doi.org/10.1038/nature10783

Doulatov, S., F. Notta, E. Laurenti, and J.E. Dick. 2012. Hematopoiesis: a human perspective. *Cell Stem Cell.* 10:120–136. http://dx.doi.org/10.1016/j.stem.2012.01.006

Ehninger, A., and A. Trumpp. 2011. The bone marrow stem cell niche grows up: mesenchymal stem cells and macrophages move in. *J. Exp. Med.* 208:421–428. http://dx.doi.org/10.1084/jem.20110132

Essers, M.A., and A. Trumpp. 2010. Targeting leukemic stem cells by breaking their dormancy. *Mol. Oncol.* 4:443–450. http://dx.doi.org/10.1016/j.molonc.2010.06.001

Essers, M.A., S. Offner, W.E. Blanco-Bose, Z. Waibler, U. Kalinke, M.A. Duchosal, and A. Trumpp. 2009. IFNalpha activates dormant haematopoietic stem cells in vivo. *Nature.* 458:904–908. http://dx.doi.org/10.1038/nature07815

Freeman, D., R. Lesche, N. Kertesz, S. Wang, G. Li, J. Gao, M. Groszer, H. Martinez-Diaz, N. Rozengurt, G. Thomas, et al. 2006. Genetic background controls tumor development in PTEN-deficient mice. *Cancer Res.* 66:6492–6496. http://dx.doi.org/10.1158/0008-5472.CAN-05-4143

Göthert, J.R., S.E. Gustin, M.A. Hall, A.R. Green, B. Göttgens, D.J. Izon, and C.G. Begley. 2005. In vivo fate-tracing studies using the Scl stem cell enhancer: embryonic hematopoietic stem cells significantly contribute to adult hematopoiesis. *Blood.* 105:2724–2732. http://dx.doi.org/10.1182/blood-2004-08-3037

Groszer, M., R. Erickson, D.D. Scripture-Adams, R. Lesche, A. Trumpp, J.A. Zack, H.I. Kornblum, X. Liu, and H. Wu. 2001. Negative regulation of neural stem/progenitor cell proliferation by the Pten tumor suppressor gene in vivo. *Science.* 294:2186–2189. http://dx.doi.org/10.1126/science.1065518

Gu, T., Z. Zhang, J. Wang, J. Guo, W.H. Shen, and Y. Yin. 2011. CREB is a novel nuclear target of PTEN phosphatase. *Cancer Res.* 71:2821–2825. http://dx.doi.org/10.1158/0008-5472.CAN-10-3399

Guo, W., J.L. Lasky, C.J. Chang, S. Mosessian, X. Lewis, Y. Xiao, J.E. Yeh, J.Y. Chen, M.L. Iruela-Arispe, M. Varella-Garcia, and H. Wu. 2008. Multi-genetic events collaboratively contribute to Pten-null leukaemia stem-cell formation. *Nature.* 453:529–533. http://dx.doi.org/10.1038/nature06933

Hasegawa, M., T.M. Baldwin, D. Metcalf, and S.J. Foote. 2000. Progenitor cell mobilization by granulocyte colony-stimulating factor controlled by loci on chromosomes 2 and 11. *Blood.* 95:1872–1874.

Henckaerts, E., H. Geiger, J.C. Langer, P. Rebollo, G. Van Zant, and H.W. Snoeck. 2002. Genetically determined variation in the number of phenotypically defined hematopoietic progenitor and stem cells and in their response to early-acting cytokines. *Blood.* 99:3947–3954. http://dx.doi.org/10.1182/blood.V99.11.3947

Henckaerts, E., J.C. Langer, J. Orenstein, and H.W. Snoeck. 2004. The positive regulatory effect of TGF-beta2 on primitive murine hemopoietic stem and progenitor cells is dependent on age, genetic background, and serum factors. *J. Immunol.* 173:2486–2493.

Juntilla, M.M., V.D. Patil, M. Calamito, R.P. Joshi, M.J. Birnbaum, and G.A. Koretzky. 2010. AKT1 and AKT2 maintain hematopoietic stem cell function by regulating reactive oxygen species. *Blood.* 115:4030–4038. http://dx.doi.org/10.1182/blood-2009-09-241000

Kalaitzidis, D., S.M. Sykes, Z. Wang, N. Punt, Y. Tang, C. Ragu, A.U. Sinha, S.W. Lane, A.L. Souza, C.B. Clish, et al. 2012. mTOR complex 1 plays critical roles in hematopoiesis and Pten-loss-evoked leukemogenesis. *Cell Stem Cell.* 11:429–439. http://dx.doi.org/10.1016/j.stem.2012.06.009

Kharas, M.G., R. Okabe, J.J. Ganis, M. Gozo, T. Khandan, M. Paktinat, D.G. Gilliland, and K. Gritsman. 2010. Constitutively active AKT depletes hematopoietic stem cells and induces leukemia in mice. *Blood.* 115:1406–1415. http://dx.doi.org/10.1182/blood-2009-06-229443

Knobbe, C.B., V. Lapin, A. Suzuki, and T.W. Mak. 2008. The roles of PTEN in development, physiology and tumorigenesis in mouse models: a tissue-by-tissue survey. *Oncogene.* 27:5398–5415. http://dx.doi.org/10.1038/onc.2008.238

Krutzik, P.O., A. Trejo, K.R. Schulz, and G.P. Nolan. 2011. Phospho flow cytometry methods for the analysis of kinase signaling in cell lines and primary human blood samples. *Methods Mol. Biol.* 699:179–202. http://dx.doi.org/10.1007/978-1-61737-950-5_9

Kühn, R., F. Schwenk, M. Aguet, and K. Rajewsky. 1995. Inducible gene targeting in mice. *Science.* 269:1427–1429. http://dx.doi.org/10.1126/science.7660125

Lander, A.D., J. Kimble, H. Clevers, E. Fuchs, D. Montarras, M. Buckingham, A.L. Calof, A. Trumpp, and T. Oskarsson. 2012. What does the concept of the stem cell niche really mean today? *BMC Biol.* 10:19. http://dx.doi.org/10.1186/1741-7007-10-19

Lapidot, T., and I. Petit. 2002. Current understanding of stem cell mobilization: the roles of chemokines, proteolytic enzymes, adhesion molecules, cytokines, and stromal cells. *Exp. Hematol.* 30:973–981. http://dx.doi.org/10.1016/S0301-472X(02)00883-4

Laterveer, L., I.J. Lindley, M.S. Hamilton, R. Willemze, and W.E. Fibbe. 1995. Interleukin-8 induces rapid mobilization of hematopoietic stem cells with radioprotective capacity and long-term myelolymphoid repopulating ability. *Blood.* 85:2269–2275.

Lee, J.Y., D. Nakada, O.H. Yilmaz, Z. Tothova, N.M. Joseph, M.S. Lim, D.G. Gilliland, and S.J. Morrison. 2010. mTOR activation induces tumor suppressors that inhibit leukemogenesis and deplete hematopoietic stem cells after Pten deletion. *Cell Stem Cell.* 7:593–605. http://dx.doi.org/10.1016/j.stem.2010.09.015

Magee, J.A., T. Ikenoue, D. Nakada, J.Y. Lee, K.L. Guan, and S.J. Morrison. 2012. Temporal changes in PTEN and mTORC2 regulation of hematopoietic stem cell self-renewal and leukemia suppression. *Cell Stem Cell.* 11:415–428. http://dx.doi.org/10.1016/j.stem.2012.05.026

Matsumoto, A., S. Takeishi, T. Kanie, E. Susaki, I. Onoyama, Y. Tateishi, K. Nakayama, and K.I. Nakayama. 2011. p57 is required for quiescence and maintenance of adult hematopoietic stem cells. *Cell Stem Cell.* 9:262–271. http://dx.doi.org/10.1016/j.stem.2011.06.014

Mei, J., Y. Liu, N. Dai, C. Hoffmann, K.M. Hudock, P. Zhang, S.H. Guttentag, J.K. Kolls, P.M. Oliver, F.D. Bushman, and G.S. Worthen. 2012. Cxcr2 and Cxcl5 regulate the IL-17/G-CSF axis and neutrophil homeostasis in mice. *J. Clin. Invest.* 122:974–986. http://dx.doi.org/10.1172/JCI60588

Miletic, A.V., A.N. Anzelon-Mills, D.M. Mills, S.A. Omori, I.M. Pedersen, D.M. Shin, J.V. Ravetch, S. Bolland, H.C. Morse III, and R.C. Rickert. 2010. Coordinate suppression of B cell lymphoma by PTEN and SHIP phosphatases. *J. Exp. Med.* 207:2407–2420. http://dx.doi.org/10.1084/jem.20091962

Nervi, B., D.C. Link, and J.F. DiPersio. 2006. Cytokines and hematopoietic stem cell mobilization. *J. Cell. Biochem.* 99:690–705. http://dx.doi.org/10.1002/jcb.21043

Orford, K.W., and D.T. Scadden. 2008. Deconstructing stem cell self-renewal: genetic insights into cell-cycle regulation. *Nat. Rev. Genet.* 9:115–128. http://dx.doi.org/10.1038/nrg2269

Palomero, T., M.L. Sulis, M. Cortina, P.J. Real, K. Barnes, M. Ciofani, E. Caparros, J. Buteau, K. Brown, S.L. Perkins, et al. 2007. Mutational loss of PTEN induces resistance to NOTCH1 inhibition in T-cell leukemia. *Nat. Med.* 13:1203–1210. http://dx.doi.org/10.1038/nm1636

Park, D., D.B. Sykes, and D.T. Scadden. 2012. The hematopoietic stem cell niche. *Front Biosci* (*Landmark Ed*). 17:30–39. http://dx.doi.org/10.2741/3913

Qian, H., N. Buza-Vidas, C.D. Hyland, C.T. Jensen, J. Antonchuk, R. Månsson, L.A. Thoren, M. Ekblom, W.S. Alexander, and S.E. Jacobsen. 2007. Critical role of thrombopoietin in maintaining adult quiescent hematopoietic stem cells. *Cell Stem Cell.* 1:671–684. http://dx.doi.org/10.1016/j.stem.2007.10.008

Song, M.S., L. Salmena, and P.P. Pandolfi. 2012. The functions and regulation of the PTEN tumour suppressor. *Nat. Rev. Mol. Cell Biol.* 13:283–296. http://dx.doi.org/10.1038/nrm3330

Sugiyama, T., H. Kohara, M. Noda, and T. Nagasawa. 2006. Maintenance of the hematopoietic stem cell pool by CXCL12-CXCR4 chemokine signaling in bone marrow stromal cell niches. *Immunity.* 25:977–988. http://dx.doi.org/10.1016/j.immuni.2006.10.016

Svensson, R.U., J.M. Haverkamp, D.R. Thedens, M.B. Cohen, T.L. Ratliff, and M.D. Henry. 2011. Slow disease progression in a C57BL/6 pten-deficient mouse model of prostate cancer. *Am. J. Pathol.* 179:502–512. http://dx.doi.org/10.1016/j.ajpath.2011.03.014

Szilvassy, S.J., R.K. Humphries, P.M. Lansdorp, A.C. Eaves, and C.J. Eaves. 1990. Quantitative assay for totipotent reconstituting hematopoietic stem cells by a competitive repopulation strategy. *Proc. Natl. Acad. Sci. USA.* 87:8736–8740. http://dx.doi.org/10.1073/pnas.87.22.8736

Tesio, M., and A. Trumpp. 2011. Breaking the cell cycle of HSCs by p57 and friends. *Cell Stem Cell.* 9:187–192. http://dx.doi.org/10.1016/j.stem.2011.08.005

Tesio, M., K. Golan, S. Corso, S. Giordano, A. Schajnovitz, Y. Vagima, S. Shivtiel, A. Kalinkovich, L. Caione, L. Gammaitoni, et al. 2011. Enhanced c-Met activity promotes G-CSF–induced mobilization of hematopoietic progenitor cells via ROS signaling. *Blood.* 117:419–428. http://dx.doi.org/10.1182/blood-2009-06-230359

Tothova, Z., and D.G. Gilliland. 2007. FoxO transcription factors and stem cell homeostasis: insights from the hematopoietic system. *Cell Stem Cell.* 1:140–152. http://dx.doi.org/10.1016/j.stem.2007.07.017

Van Zant, G., P.W. Eldridge, R.R. Behringer, and M.J. Dewey. 1983. Genetic control of hematopoietic kinetics revealed by analyses of allophenic mice and stem cell suicide. *Cell.* 35:639–645. http://dx.doi.org/10.1016/0092-8674(83)90096-X

Vivanco, I., N. Palaskas, C. Tran, S.P. Finn, G. Getz, N.J. Kennedy, J. Jiao, J. Rose, W. Xie, M. Loda, et al. 2007. Identification of the JNK signaling pathway as a functional target of the tumor suppressor PTEN. *Cancer Cell.* 11:555–569. http://dx.doi.org/10.1016/j.ccr.2007.04.021

Wilson, A., M.J. Murphy, T. Oskarsson, K. Kaloulis, M.D. Bettess, G.M. Oser, A.C. Pasche, C. Knabenhans, H.R. Macdonald, and A. Trumpp. 2004. c-Myc controls the balance between hematopoietic stem cell self-renewal and differentiation. *Genes Dev.* 18:2747–2763. http://dx.doi.org/10.1101/gad.313104

Wilson, A., E. Laurenti, G. Oser, R.C. van der Wath, W. Blanco-Bose, M. Jaworski, S. Offner, C.F. Dunant, L. Eshkind, E. Bockamp, et al. 2008. Hematopoietic stem cells reversibly switch from dormancy to self-renewal during homeostasis and repair. *Cell.* 135:1118–1129. http://dx.doi.org/10.1016/j.cell.2008.10.048

Winkler, I.G., N.A. Sims, A.R. Pettit, V. Barbier, B. Nowlan, F. Helwani, I.J. Poulton, N. van Rooijen, K.A. Alexander, L.J. Raggatt, and J.P. Lévesque. 2010. Bone marrow macrophages maintain hematopoietic stem cell (HSC) niches and their depletion mobilizes HSCs. *Blood.* 116:4815–4828. http://dx.doi.org/10.1182/blood-2009-11-253534

Xu, P.Z., M.L. Chen, S.M. Jeon, X.D. Peng, and N. Hay. 2012. The effect Akt2 deletion on tumor development in Pten(+/-) mice. *Oncogene.* 31:518–526. http://dx.doi.org/10.1038/onc.2011.243

Yamazaki, S., A. Iwama, S. Takayanagi, Y. Morita, K. Eto, H. Ema, and H. Nakauchi. 2006. Cytokine signals modulated via lipid rafts mimic niche signals and induce hibernation in hematopoietic stem cells. *EMBO J.* 25:3515–3523. http://dx.doi.org/10.1038/sj.emboj.7601236

Yamazaki, S., H. Ema, G. Karlsson, T. Yamaguchi, H. Miyoshi, S. Shioda, M.M. Taketo, S. Karlsson, A. Iwama, and H. Nakauchi. 2011. Nonmyelinating Schwann cells maintain hematopoietic stem cell hibernation in the bone marrow niche. *Cell.* 147:1146–1158. http://dx.doi.org/10.1016/j.cell.2011.09.053

Yilmaz, O.H., R. Valdez, B.K. Theisen, W. Guo, D.O. Ferguson, H. Wu, and S.J. Morrison. 2006. Pten dependence distinguishes haematopoietic stem cells from leukaemia-initiating cells. *Nature.* 441:475–482. http://dx.doi.org/10.1038/nature04703

Yoshihara, H., F. Arai, K. Hosokawa, T. Hagiwara, K. Takubo, Y. Nakamura, Y. Gomei, H. Iwasaki, S. Matsuoka, K. Miyamoto, et al. 2007. Thrombopoietin/MPL signaling regulates hematopoietic stem cell quiescence and interaction with the osteoblastic niche. *Cell Stem Cell.* 1:685–697. http://dx.doi.org/10.1016/j.stem.2007.10.020

Yu, H., Y. Yuan, H. Shen, and T. Cheng. 2006. Hematopoietic stem cell exhaustion impacted by p18 INK4C and p21 Cip1/Waf1 in opposite manners. *Blood.* 107:1200–1206. http://dx.doi.org/10.1182/blood-2005-02-0685

Zhang, J., J.C. Grindley, T. Yin, S. Jayasinghe, X.C. He, J.T. Ross, J.S. Haug, D. Rupp, K.S. Porter-Westpfahl, L.M. Wiedemann, et al. 2006. PTEN maintains haematopoietic stem cells and acts in lineage choice and leukaemia prevention. *Nature.* 441:518–522. http://dx.doi.org/10.1038/nature04747

Zou, P., H. Yoshihara, K. Hosokawa, I. Tai, K. Shinmyozu, F. Tsukahara, Y. Maru, K. Nakayama, K.I. Nakayama, and T. Suda. 2011. p57(Kip2) and p27(Kip1) cooperate to maintain hematopoietic stem cell quiescence through interactions with Hsc70. *Cell Stem Cell.* 9:247–261. http://dx.doi.org/10.1016/j.stem.2011.07.003